Supplementary Material

GABAergic circuits control stimulus-instructed receptive field development in the optic tectum

Blake A. Richards, Oliver P. Voss & Colin J. Akerman

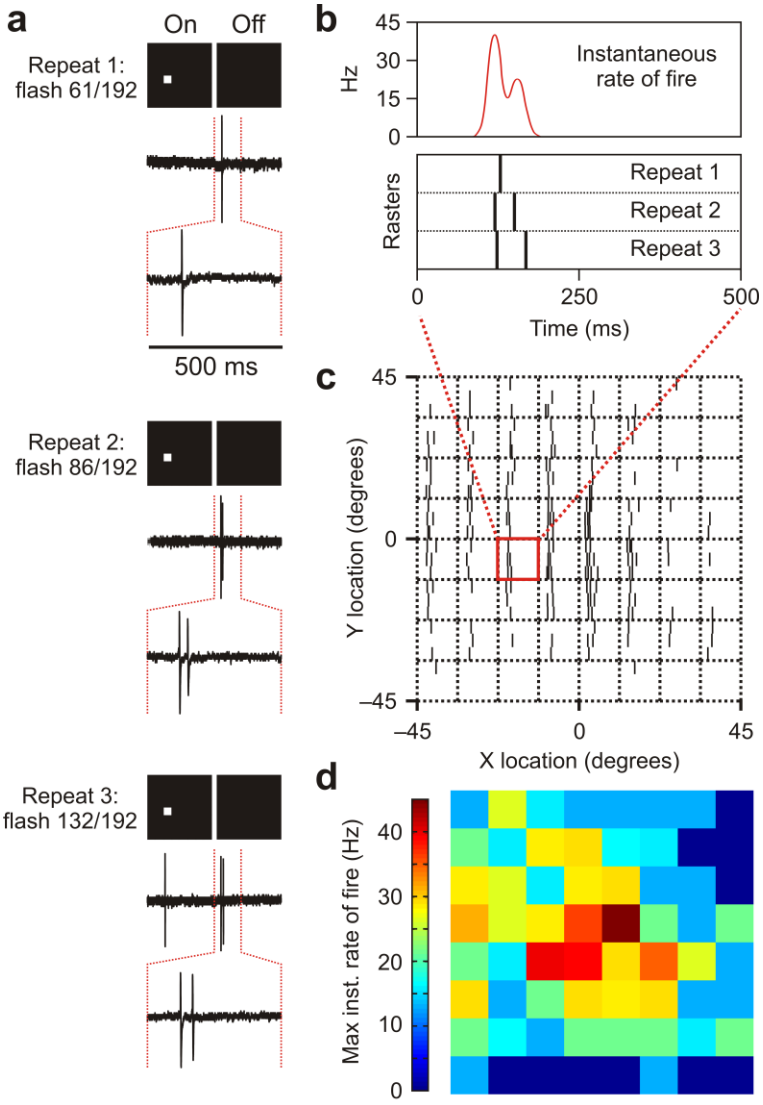

Supplementary Figure 1
The receptive field mapping protocol for tectal neurons. **(a)** Continuous loose-patch cell attached recordings of individual tectal neurons were made during presentation of stimuli. The stimuli consisted of small white squares flashed in different locations of the screen. Each square occupied one location of an 8 x 8 grid, giving a total of 64 different locations. The flashed stimuli occurred at a rate of 0.4 Hz. The stimuli were presented so that each location was repeated 3 times in a pseudorandom order, producing a total of 192 flashes. In the examples shown here (taken from one cell), a location just left and below the center of the screen was selected on the 61st, 86th, and 132nd flashes. The cell's action potential activity in the first 500 ms following the disappearance of the squares was used to quantify the cell's receptive field. **(b)** Spikes were detected and raster plots of the 3 repeats were generated. The raster plot for the responses shown in (a) is illustrated here (bottom). These raster plots were then used to estimate the instantaneous rate of fire, illustrated by the red trace (top). **(c)** The raster plots of the responses at each location were laid out in a visuotopic map. Note the clear spatial structure of this cell's responses to flashes in different locations. **(d)** The maximum instantaneous rate of fire for each raster was estimated, and used to construct a color-coded map of the responses to each area. These scalar maps provided a quantifiable measurement of the spatial structure of the cells' receptive fields.

Nature Neuroscience: doi:10.1038/nn.2612

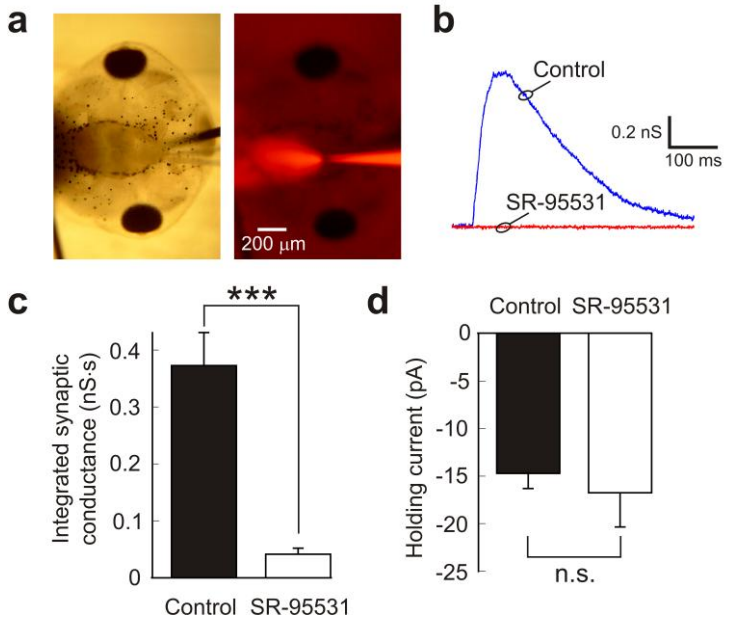

Supplementary Figure 2 Blocking GABA-A receptors in tectal neurons.
(a) ACSF containing 50 µM SR-95531 was administered locally to the optic tectum via a glass pipette using constant air pressure. A red fluorescent dye was included in the solution to allow for monitoring of flow. Photograph shows local application to the optic tectum of a stage 43 tadpole. **(b)** SR-95531 application abolished visually-evoked GABAergic synaptic conductances recorded at the glutamatergic reversal potential in whole-cell voltage-clamp mode. **(c)** The conductances evoked by the receptive field mapping protocol during SR-95531 application (n = 10 cells) were found to be close to zero and highly significantly reduced in comparison to control cells (n = 31 cells). Data shown is median with 95% C.I. (***$P < 0.001$, Mann-Whitney *U*-test). **(d)** During whole-cell recordings the holding current at -60 mV showed no significant difference between control and SR-95531 cells. Data shown is mean ± s.e.m. ($P = 0.56$, *t*-test).

Nature Neuroscience: doi:10.1038/nn.2612

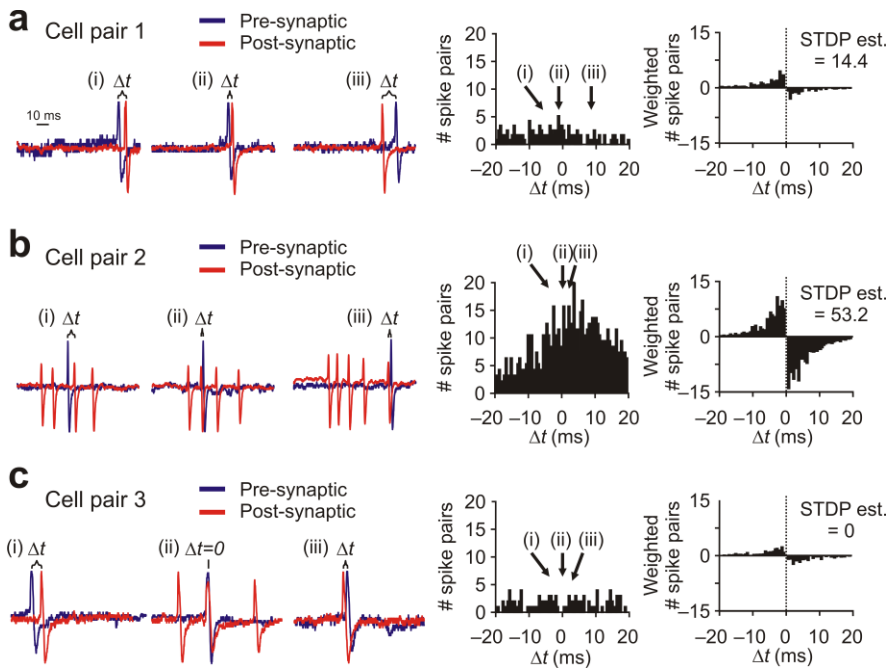

Supplementary Figure 3 Calculating Monte-Carlo estimates of tectal-tectal STDP.
(a-c) Pairs of tectal cells were randomly sampled from the population of recorded cells and the cells within each pair were then randomly assigned as "presynaptic" or "postsynaptic". Using the data recorded during presentation of the training stimulus, presynaptic (blue) and postsynaptic (red) spike pairs were randomly sampled from each cell pair. Three example spike pairs are shown for three different cell pairs (left). For each cell pair the difference in time between the spikes, Δ*t*, was used to construct a histogram of spike-time differences (center). This histogram was then weighted with a STDP function (right)[49]. The absolute value of the sum of the weighted histogram provided the STDP estimate and reflected the bias for spike pairs to generate either LTP or LTD within the STDP window. The spike pairs sampled from the 1st cell pair (a) exhibited a tendency for presynaptic spikes to precede postsynaptic spikes and therefore the STDP estimate for this cell was moderately high. The spike pairs sampled from the 2nd cell pair (b) showed a strong tendency for postsynaptic spikes to occur before presynaptic spikes and this generated a large STDP estimate for this cell pair. In contrast, spike pairs sampled from the 3rd cell pair (c) exhibited no tendency for either cell's spikes to come first, and so produced an STDP estimate of 0.

Nature Neuroscience: doi:10.1038/nn.2612

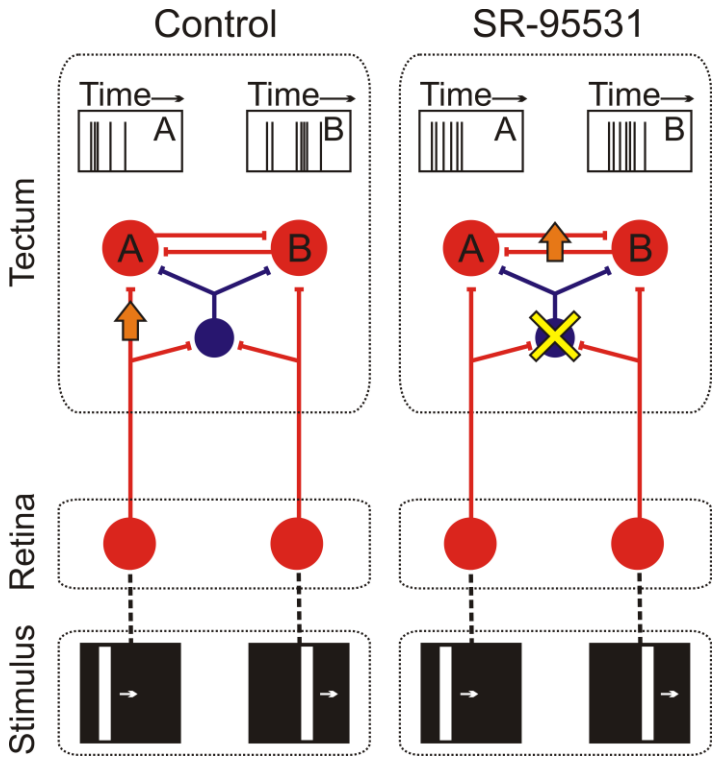

Supplementary Figure 4 A conceptual model of the developing optic tectum during presentation of a moving stimulus.
Under control conditions (left) tectal cells receive GABAergic inputs (blue) and glutamatergic inputs (red)[29]. The model postulates that as a stimulus moves through visual space (bottom) GABAergic inputs to different tectal cells (A and B) will arrive at different times relative to the glutamatergic inputs. For example, when the stimulus is in the left part of visual space, cell A will receive a rapid monosynaptic glutamatergic input followed by a disynaptic GABAergic input, whereas cell B will receive polysynaptic glutamatergic input and GABAergic input at overlapping times. This could enhance differences in the spike times of cells A and B, and reduce tectal-tectal spike-timing correlations (raster plots at top). Therefore the most robust correlations between presynaptic and postsynaptic spike-timing (orange arrows) are those driven by retinal input, which presumably most closely reflect the statistics of the stimulus. Under GABA blockade (right) stimulation of the left part of visual space produces glutamatergic inputs to cells A & B that are no longer affected by GABAergic inputs arriving at different times. In this scenario the spiking patterns of the two tectal cells are much more similar (raster plots at top) and contain significant correlations that are weakly related to the statistics of the stimulus. In this situation plasticity could be dominated by other factors, such as recurrent connectivity, and the system would be less able to exhibit learning that reflects the properties of the stimulus.

Nature Neuroscience: doi:10.1038/nn.2612

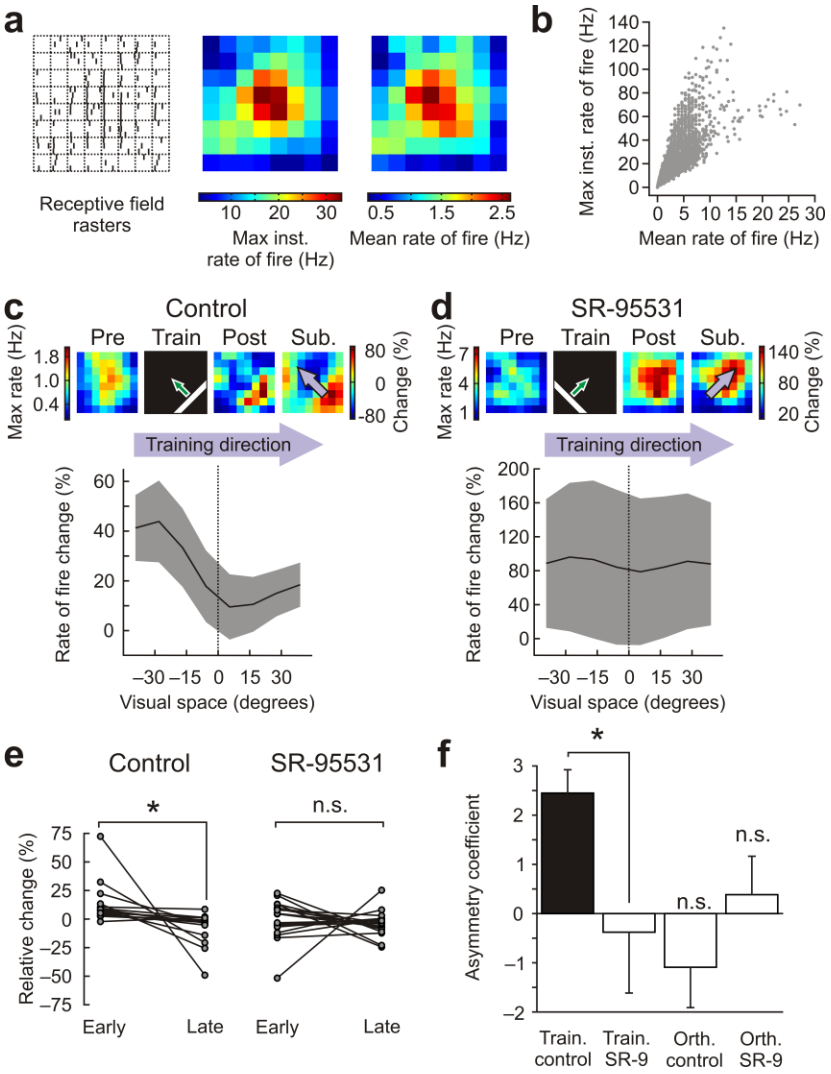

Supplementary Figure 5
Measurement of receptive fields using mean rate of fire shows instructive learning in control conditions but not under GABA-A receptor blockade.
(a) Throughout the manuscript receptive field maps were generated using maximum instantaneous rate of fire. Receptive fields were similar when they were generated using mean rate of fire instead (i.e. the number of spikes divided by the length of time). An example cell's raster plot and receptive field maps measured using the two different values are shown. **(b)** There was a significant correlation between the mean rate of fire and the maximum instantaneous rate of fire across all receptive field locations and all cells (Pearson's $r = 0.84$, $P < 0.001$). **(c)** When receptive fields were analyzed using mean rate of fire the control cells showed asymmetric training effects in the direction of training (n = 18 cells). An example cell is shown at the top and population data is shown as mean ± s.e.m (shaded region). **(d)** Receptive field maps measured by mean rate of fire for SR-95531 cells did not exhibit instructive effects, but flat potentiation across the field, shown by an example cell and for the population (n = 19 cells). **(e)** Changes around the center of the receptive fields measured using mean rate of fire exhibited significant asymmetric training effects in control cells but not in SR-95531 cells (*$P < 0.05$, paired *t*-test). **(f)** Asymmetry coefficients calculated using mean rate of fire maps were significantly different from 0 for control cells in the direction of training, but not for SR-95531 cells, or for either group in the orthogonal direction. Data shown is mean ± s.e.m.

Nature Neuroscience: doi:10.1038/nn.2612

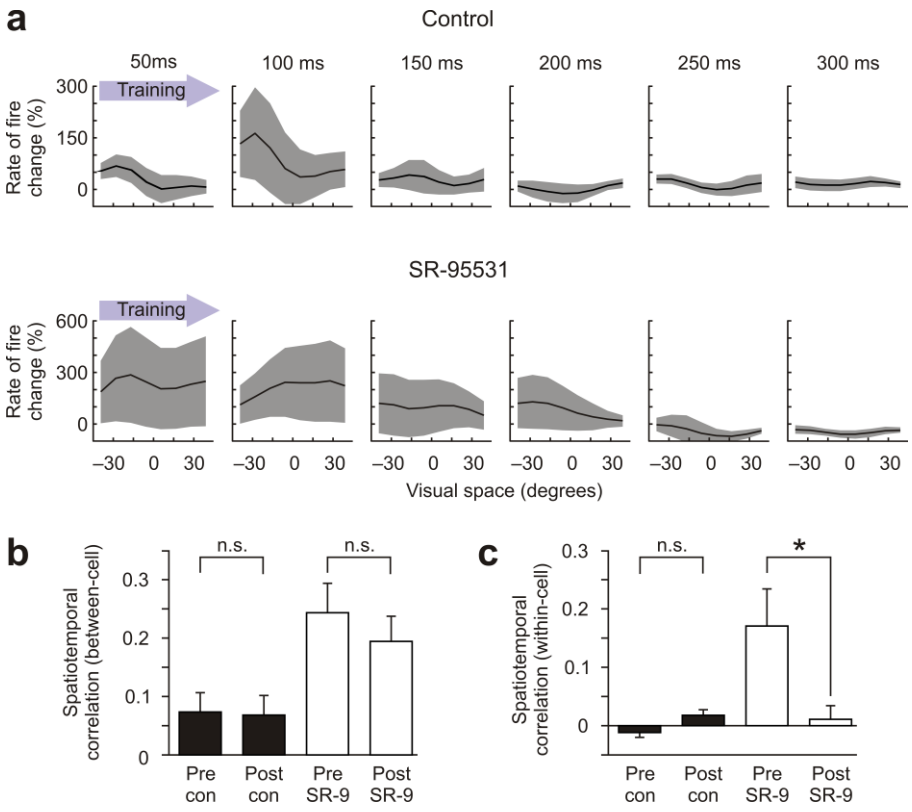

Supplementary Figure 6 Effects of training on spatiotemporal responses.
(a) Changes in spatiotemporal responses following training were examined in cells where it had been possible to collect a high number of repeats with the receptive field mapping protocol (n = 7 control cells, n = 6 SR-95531 cells). As shown in Figure 3, asymmetric effects from training were clear in control cells but not SR-95531 condition cells. This is illustrated here by plots showing the mean change in responses for distinct latency time-bins (differences in the direction of training are shown, data is mean ± s.e.m.). Changes in the responses of control cells were primarily restricted to earlier latencies, but there was a trend towards comparatively later changes in responses in the GABA blocked cells. **(b)** Between-cell correlations in the spatiotemporal responses for the two groups were examined before and after training (see Online Methods). Control cells showed almost no differences in their correlations before and after training. SR-95531 cells showed a non-significant trend towards less correlation. Data shown is mean ± s.e.m. **(d)** Within-cell correlations in the spatiotemporal responses following training were not significantly different for control cells, but were significantly lower for SR-95531 cells. Data shown is mean ± s.e.m. (*P < 0.05, one-way ANOVA with Bonferroni corrected post-hoc comparisons).

Nature Neuroscience: doi:10.1038/nn.2612

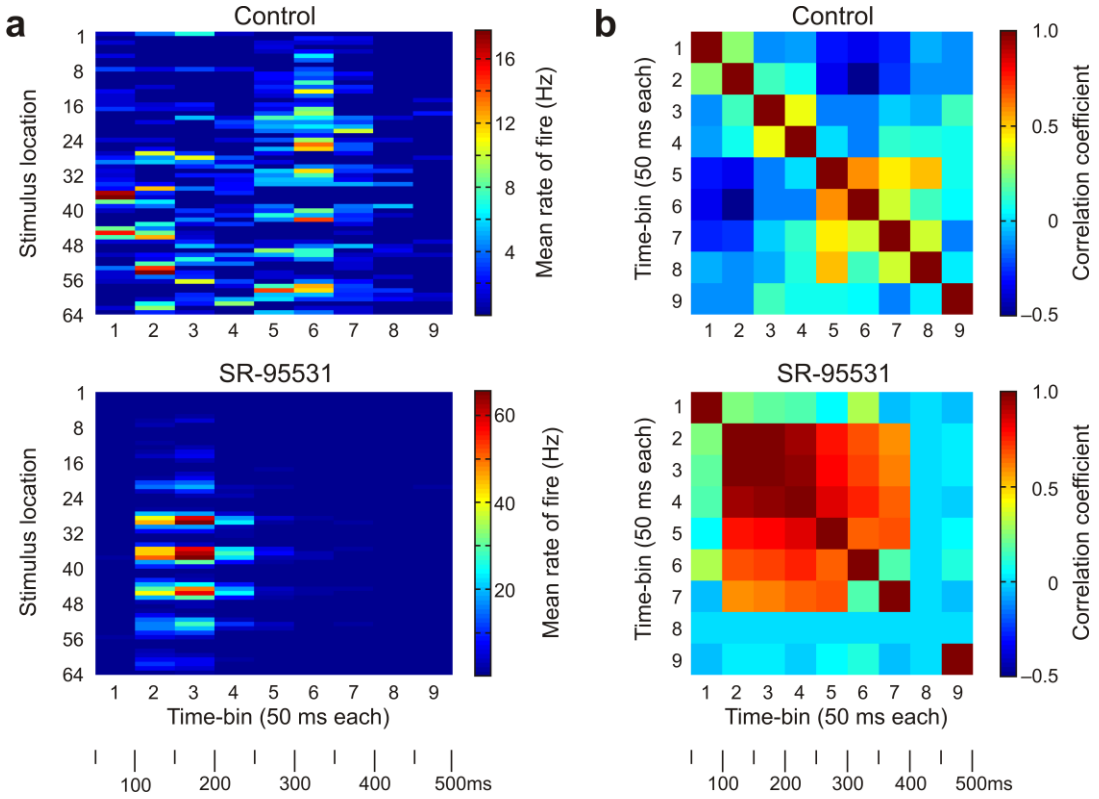

Supplementary Figure 7 Calculation of within-cell correlations in spatiotemporal responses. **(a)** To measure the correlation within the cells' spatiotemporal responses the 3D spatiotemporal data (8 locations x 8 locations x 9 post-stimulus time bins) was treated as 9 different vectors each containing 64 locations. This is shown by examples for two cells here, one in the control condition (top) and one recorded during SR-95531 application (bottom). The maps lay out all 64 positions in stimulus space vertically from the top left stimulus location on the projection screen ('1') to the bottom right stimulus location ('64'). The color indicates the neuron's mean rate of fire elicited by a stimulus at that location, laid out horizontally for each post-stimulus time bin. **(b)** Correlation coefficient matrices for the spatiotemporal maps shown in (a). Each pixel in the matrix represents the correlation coefficient across all 64 stimulus locations for two time bins. High positive correlation coefficients indicate that spikes during those two post-stimulus time bins were triggered by stimuli at similar locations of the receptive field. The within-cell spatiotemporal correlation was measured as the average of the 36 unique correlation coefficients for that cell's spatiotemporal response map.

Nature Neuroscience: doi:10.1038/nn.2612